An apparatus to measure frictional, anelastic, and viscous behavior in ice at temperate and planetary conditions

C. McCarthy,[a] H. M. Savage, T. Koczynski, and M. A. Nielson
Lamont-Doherty Earth Observatory, Columbia University, Palisades, New York 10964, USA

(Received 16 November 2015; accepted 2 May 2016; published online 31 May 2016)

In this paper, we describe a cryogenic, servo-controlled biaxial friction apparatus designed to measure the deformational behaviors of ice. The apparatus is specifically designed to accurately achieve and measure the low differential stresses applicable to deforming ice on earth and on icy satellites. We can apply loads in the range ~2–1800 kPa and velocities up to 4 mm/s, with resolution of 39 Pa and 0.7 μm, respectively. Precise temperature control, measurement, and insulation allow testing at constant temperature (from −2 to −30 °C) for prolonged periods of time. The apparatus is tested with various plastics as well as with polycrystalline ice samples and the results are consistent with previously published values. Critical components of the instrument are described along with examples of data collection schemes and preliminary results. The flexibility of the design allows for both glaciological and planetary applications over a range of deformational behaviors including friction, anelastic, and viscous. *Published by AIP Publishing.* [http://dx.doi.org/10.1063/1.4950782]

I. INTRODUCTION

A growing body of literature documents the importance of non-steady state behavior of deforming ice in terrestrial glaciers and ice streams, as well as on icy satellites like Europa and Enceladus. Deformation in these icy settings is likely a combination of frictional, anelastic, and viscous processes. To study these phenomena, we designed and built a servo-controlled ice deformation apparatus equipped with a programmable cryostat. The design is flexible, so that ice friction, creep, and attenuation experiments are possible. In particular, the ability to study the friction of ice-on-ice, ice-on-rock (or a till layer), and ice mixtures (including various salts) will provide important physical parameters for studies of ice deformation in both Earth and planetary contexts.

A. Observations

1. Glaciers and ice streams

Models of ice mass balance and sea level rise are dependent in part on the rate that ice is transported from accumulation zones to the oceans. The factors that determine flow rates within the bulk of the ice and sliding rates at the ice-bedrock interface are poorly understood. Glacier motion is controlled by various processes from friction to ductile flow, and possibly by anelasticity (e.g., Gudmundsson (2007)). The dominant mode of deformation may depend on the time scale of loading. For instance, many tidewater ice streams have flow rates that are modulated by the ocean tides (e.g., Adalgeirsdottir *et al.*, 2008; deJuan *et al.*, 2010; Wiens *et al.*, 2008; Winberry *et al.*, 2009; Winberry *et al.*, 2011; and Zoet *et al.*, 2012). The sensitive glacier response to well-known, periodic, tidal forcing raises the possibility of using glacier response to infer key glacier properties. However, much is unknown about the physics of glacier tidal response, which can be quite large despite the small size of the tidal signal, or how strain is partitioned between bulk versus basal deformation. This apparatus allows us to measure the frictional and viscoelastic behaviors of ice, which we will compare to observational data and theoretical predictions to better understand the physics of ice flow.

2. Icy satellites

Measuring the frictional response of ice is also important for understanding icy satellite behavior. Both the viscoelastic and frictional responses may play an important role in tidal heating and convection on bodies like Enceladus and Europa. Frictional heating produced by loading of faults on icy satellites may be sufficient to create localized melting to account for observed geysers at fractures on these moons (Nimmo *et al.*, 2007). Localized frictional heating has also been posited as a cause for reduced friction coefficients that explain long run out landslides on Iapetus (Singer *et al.*, 2012). However, ice friction at the low temperatures of icy satellites (T = 100–200 K) has received very little attention. With this apparatus we will be able to measure friction of ice-on-ice at low temperatures to explore frictional strength and fault healing at very low sliding rates consistent with tidal loading of faults.

B. Background

1. Friction of ice

Previous work on ice friction has demonstrated a strong dependence on temperature, pressure, and sliding rate (Barnes *et al.*, 1971). Three velocity-dependent friction domains have been noted, where friction is highest at intermediate velocities and falls at the lowest and highest velocities. Frictional melt is thought to be a significant weakening mechanism above

[a]Author to whom correspondence should be addressed. Electronic mail: mccarthy@ldeo.columbia.edu.

$\sim 10^{-3}$ m/s slip rates (Barnes *et al.*, 1971; Bowden and Hughes, 1939; Kennedy *et al.*, 2000; and Maeno *et al.*, 2003), whereas creep is thought to contribute to low friction at slow rates (Bowden and Hughes, 1939 and Schulson and Fortt, 2012). Intermediate speeds ($\sim 10^{-5}$–10^{-4} m/s) have the highest friction and are thought to be dominated by fracture (Kennedy *et al.*, 2000).

Other studies have focused on other compositions of ice. Although saline ice has a lower friction coefficient than freshwater ice at low temperatures, it also displays velocity weakening behavior at higher velocities, as freshwater ice does (Kennedy *et al.*, 2000 and Lishman *et al.*, 2011). Zoet *et al.* (2013) showed that increasing ice debris (in the form of natural and synthetic rock particles) can increase coefficient of friction and influence the transition from velocity strengthening to velocity weakening behavior.

Only recently have studies looked at ice friction within the context of rate-and-state friction (Zoet *et al.*, 2013). Frictional sliding on interfaces such as the base of glaciers and fault surfaces is governed by both the sliding velocity and the slip history, which are related through the rate-and-state friction laws (Dieterich, 1972; Ruina, 1983; and Marone, 1998). The rate-and-state friction law states that friction is a function of both the sliding velocity and the asperity contact memory,

$$\mu = \mu_0 + a \ln\left(\frac{V}{V_0}\right) + b \ln\left(\frac{\theta V_0}{D_C}\right), \tag{1}$$

where μ is friction, μ_0 is the reference friction at the reference velocity V_0, V is sliding velocity, D_c is the critical slip distance required to renew asperity contacts, θ is the state variable that is equal to D_c/V at steady state, and a and b are empirically derived friction parameters. The evolution of the state variable has been described both with evolution at near zero velocity (Dieterich, 1972),

$$\frac{d\theta}{dt} = 1 - \frac{V\theta}{D_c} \tag{2}$$

or with evolution that depends more on slip (Ruina, 1983),

$$\frac{d\theta}{dt} = -\frac{V\theta}{D_c} \ln\left(\frac{V\theta}{D_c}\right). \tag{3}$$

The application of rate-and-state friction theory to settings with oscillating loads such as seismic waves and tides has led to interesting observations of critical behavior of frictional properties in rocks controlled by the amplitude and frequency of loading (Lockner and Beeler, 1999; Beeler and Lockner, 2003; Savage and Marone, 2007; Savage and Marone, 2008; and Van der Elst and Savage, 2015). Our new apparatus will be capable of interrogating this behavior in ice through cyclically loaded cryo-friction experiments.

2. Anelastic and viscous properties of ice

The apparatus is also capable of measuring the viscous and anelastic properties of ice (and ice mixtures) via constant load creep and cyclic loading attenuation experiments, respectively. Although much is known about the viscosity of ice at temperate conditions (e.g., Duval *et al.*, 1983) and planetary conditions (e.g., Goldsby and Kohlstedt, 2001 and Durham *et al.*, 2001), much less is known about the creep behavior of ice mixtures relevant to icy satellites, including various salts, acids, and alkanes (Durham *et al.*, 2005; McCarthy *et al.*, 2011; and Golding *et al.*, 2013). Here we will provide results from a preliminary creep test on polycrystalline ice to demonstrate that measurement of the viscous properties of ice is possible with this apparatus. The anelastic properties of ice (as well as ice mixtures) are also still poorly understood. The anelastic behavior of an icy body is its ability to turn periodic mechanical energy (from tides for instance) into heat. Tidal dissipation has recently become a focus in planetary science as a potential heat source sufficient to create and maintain subsurface global oceans (e.g., Shoji *et al.*, 2013). Laboratory experiments have shown that dissipation in polycrystalline ice involves a combination of dislocation and grain boundary processes (Tatibouet *et al.*, 1987; Cole, 1995; and McCarthy and Cooper, 2016). However, the partitioning of energy dissipation between the two mechanisms and the scaling with background stress, grain size, and strain/dislocation density are not yet known. With minor additions to the driving program, we will be able to apply sinusoidal loads that will allow these types of uniaxial, cyclic-loading experiments to be performed in future studies.

II. THE APPARATUS

Figure 1 presents a schematic illustration of the cryogenic deformation apparatus. Friction of ice sliding against rock, metal, or other ice(s) is realized in a double direct shear configuration in which two stationary blocks are held on either side of a moving inner ice block with planar and parallel faces. The inner block is pushed down vertically by a servo-controlled hydraulic piston acting on a steel plate mounted from above. A smaller horizontal hydraulic piston pushing against a fixed piston applies the load normal to the sliding surfaces. This direct shear configuration has been used successfully in studies of rock friction over the last half century (e.g., Dieterich, 1972 and Hoskins *et al.*, 1968). Steel-reinforced aluminum plates with tie rods provide the framework for the apparatus. Based on a calculation of bending in the applicable plates, the frame can hold a maximum force of 123.7 kN in the vertical direction and 35.6 kN in the horizontal direction. The apparatus sits on a strut channel frame that is mounted to a concrete pier that is anchored into bedrock. Detailed explanations of the hydraulic loading system, load and displacement measurement, temperature control, sample assembly, and data acquisition and analysis are given below.

A. Hydraulics/control

The apparatus is powered by a 40 LPM, 20 hp, 20 MPa hydraulic power supply. Both the vertical and horizontal loads are provided by servo-controlled hydraulic pistons. The hydraulic pistons can work in either load or displacement control and can be programmed to apply a constant, ramped, or periodic form. Displacement control resolution is 0.7 μm for each axis

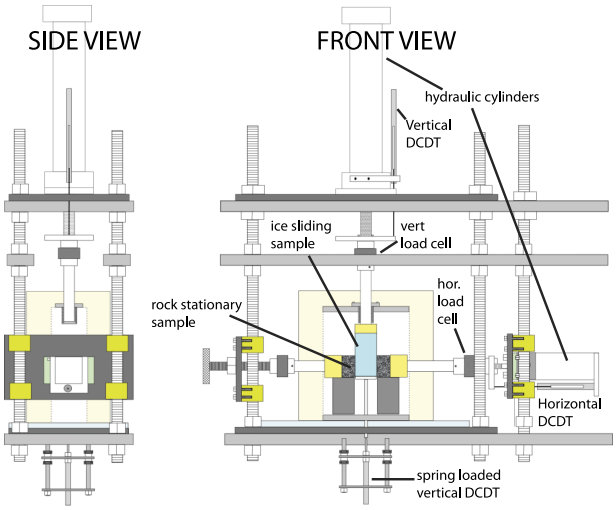

FIG. 1. Schematic illustration of cryogenic biaxial friction apparatus developed in this study.

and stress resolution is 39 Pa. Servo-controlled load point displacement rates of 1 μm/s to ~4 mm/s are possible. The stroke of the vertical piston is 304.8 mm, the bore is 63.5 mm, and the maximum push force (at 2750 psi) is 60 046 N. The stroke of the horizontal piston is 76.2 mm, the bore is 38.1 mm, and the maximum push force (at 2750 psi) is 21 614 N.

B. Measurement

Vertical load (that resolves as shear stress) and horizontal load (that resolves as normal stress) are measured by a total of three commercial load cells (Transducer Techniques, 454 kg maximum). A single load cell placed between the vertical piston and the sliding sample provides the vertical load feedback. Two load cells placed on either side of the stationary samples, one attached to the horizontal piston and one attached to a fixed piston, provide the horizontal load feedback. The output of the vertical load cell is conditioned by instrumentation amplifiers with a front panel choice in gain between high sensitivity/low stress or low sensitivity/high stress. Record channels are amplified to give 10 V full scale (or ±10 V full scale if warranted).

Vertical displacement is measured via two transducers. One is a direct current differential transformer (DCDT) with a 100 mm linear range (Schaevitz 2000 DC) to measure gross position within the rig and provides feedback to the hydraulic servo valves. The DCDT cylinder is mounted to the frame and the core is connected to a steel plate attached to the end of the vertical hydraulic piston. The other is spring-loaded DCDT (Macro sensors GHSD 750-1000) with 50 mm linear range to measure the sample movement during sliding. It is mounted from below (Figure 1). Horizontal displacement is measured by a DCDT (Macro Sensors DC-750-1000) with a 50 mm linear range. All load cells and DCDTs are positioned outside the cryostat.

C. Temperature control

Two methods of temperature control are employed depending on the conditions needed. For relatively warm temperatures consistent with terrestrial glaciers (−30 °C–0 °C), an aluminum box ($20 \times 27 \times 7.5$ cm; total mass = 3.4 kg; thermal conductivity = 167 W m^{-1} K^{-1}) is chilled by circulating a methanol-water mixture through aluminum cooling blocks ($122 \times 42 \times 12$ mm) attached to each side by quick release toggles. A thin layer of micronized silver gel is applied to each side to maximize contact and thermal transfer. The cryostat is insulated with a shell made of expanding foam. The lowest temperature that can be reached by this method alone is

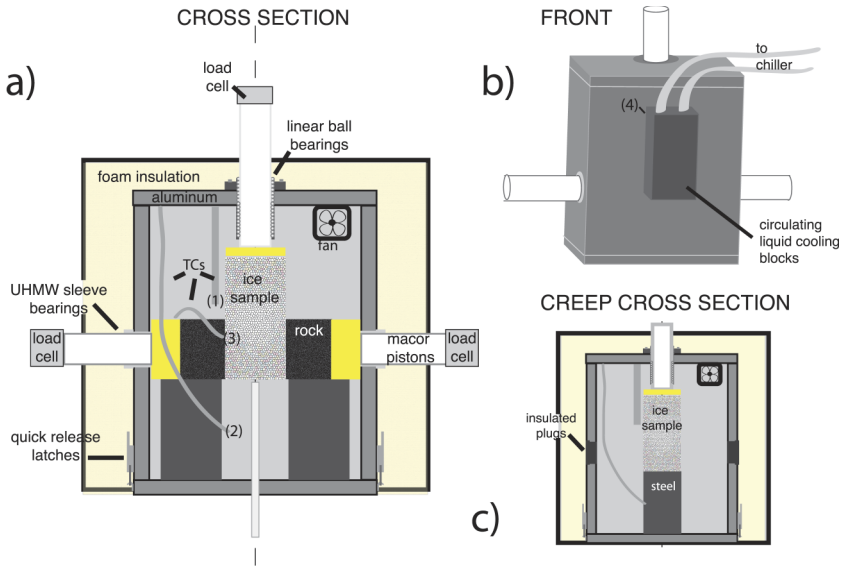

FIG. 2. Schematic of the cryostat and load trains (vertical and horizontal) (a) in cross section, showing the double direct shear configuration of the testing sample and two stationary samples, (b) in three-dimensional view to show the circulating liquid cooling mechanisms, and (c) the modification made to accommodate preliminary creep experiments. Thermocouple tip positions are labeled: (1) above the sample; (2) below the sample; (3) at the interface embedded in the rock; and (4) on the inside walls of the cryostat adjacent to the cooling blocks.

−30 °C. Multiple Type T thermocouples are positioned within the cryostat (as shown in Fig. 2) to measure the temperature: (1) above the sample; (2) below the sample; (3) at the interface embedded in the rock; and (4) on the inside walls of the cryostat adjacent to the cooling blocks. Each thermocouple has a zero point compensation provided by a thermocouple-to-analog converter (Omega TAC80B) with bias resistors for floating inputs. Manufacturer's error for Type T thermocouples is listed at ±1.8 °C. Sublimation is a concern with ice held at relatively warm temperatures for long periods of time. However with the short duration of these initial experiments (~40 min), it was not an issue. In future, longer duration experiments sublimation may need to be addressed.

For much colder temperatures consistent with planetary conditions (−30 °C to −90 °C), a different cryostat will be used that is cooled with circulating fluid traveling instead through a liquid nitrogen-cooled chamber. A solenoid valve will control the flow of the liquid nitrogen in response to a set point. Instead of exterior cooling blocks, the chilled liquid will pass through copper tubes inside the box very near to the sample. This cryostat is currently under construction.

A 12.7 mm thick insulating layer of rigid high-density polyethylene with low thermal conductivity (0.45-0.52 W/mK) separates the cryostat from the rest of the frame. During initial tests, multiple thermocouples were placed throughout the apparatus to monitor temperatures of DCDTs and load cells during testing, with no detectible change in temperature above or below room temperature.

D. Data acquisition

The voltage signals for all measurements are collected by a 32-channel 16-bit data acquisition system (National Instruments) at a maximum sampling rate of 250 kHz per channel.

E. Sample assembly

Figure 2 shows the load train in two directions for the central sliding sample. In the horizontal direction, the piston, which acts against a 1.3 cm thick steel plate, is attached by screw to a load cell that is held to a 2.5 cm OD Macor™ ceramic piston that fits snugly into a brass sample holder. (Macor™ was chosen for its low thermal conductivity, 1.46 W/mK at 25 °C). The sample holder presses against a polished rock sample (50 × 50 × 30 mm). A mirror image of this load train is on the other side of the sample attached to a stationary screw through a steel plate. The rock samples sit on steel support blocks that act to prevent rotational motion induced by direct shear. The steel blocks are bolted directly to the cryostat base and the tops are coated with dry molybdenum powder to ensure a frictionless sliding surface. Sitting between the two stationary rock samples is the slider sample. When placing the sample, the slider block is held in its uppermost position (Fig. 2) by the clamping action of plastic (ultrahigh molecular weight polyethylene, UHMW) guiderails built into the cryostat. Once normal stress is applied, the pressure provided by the guiderails is released. The vertical load train consists of the hydraulic piston, a load cell mount plate, a load cell, and a central ceramic piston. A maximum shear displacement of 50 mm is attainable with this configuration. The nature of this double-direct shear configuration, with vertical sliding interfaces, is that if melt is created during sliding, it will vacate and be a fully drained interface. If fluid pressure is the subject of a future study, the open, flexible design of this biaxial apparatus allows for a change in configuration to a horizontal sliding interface with controlled water pressure.

Samples of so-called "standard ice" (Cole, 1979 and Durham *et al.*, 1983) were prepared by packing sieved bubble-free seed ice (between 107 μm and 250 μm sieves) into a rectangular aluminum mold. Sieving and packing were conducted in a cold room (−17 °C). A packed mold was connected to a squeeze bottle of deionized, degassed water. This assembly was then immersed in a circulating ice/water bath (0 °C) for at least 25 min (a time sufficient for the center of the seed ice to reach equilibrium, as determined previously by embedding a thermocouple into a packed mold). During this time a vacuum was applied (<3 kPa) to the sealed mold to evacuate air from the pore space. After the equalization period was reached, a flow control valve between the bottle of water and the mold allowed the water to flood the evacuated pore space of the seed ice. The flooding rate is lower than the displacement rate of the vacuum pump, so the vacuum was maintained during the entirety of the flooding process, ~15 min. The mold was then placed in a freezer maintained at −5 °C atop a copper plate with insulation placed around the side and top so that freezing proceeded from the bottom up. Samples were maintained at this temperature for greater than 48 h. This method and subsequent grain growth produced rectangular samples with randomly oriented crystals of uniform size 1500 ± 280 μm in diameter with <1% porosity, as determined by micro-structural analysis (Fig. 3) using Fiji image analysis software (Schindelin *et al.*, 2012 and Schneider *et al.*, 2012). To remove samples, molds were placed in a room temperature bath for ~2 min which allowed the samples to be easily removed without needing any internal coating/greasing. The as-molded rectangular specimens were intentionally oversized (52 × 70 × 108 mm) to account for the small amount of melt created during removal. Once removed, they were shaved down with a microtome to 50 × 50 × 100 mm.

Roughness of the ice sliding surface was controlled by abrading the ice on a #100 grit piece of sandpaper within a cold room. A profilometer (Mitutoyo SF-210 calibrated against a standard) was used to characterize the microtomed

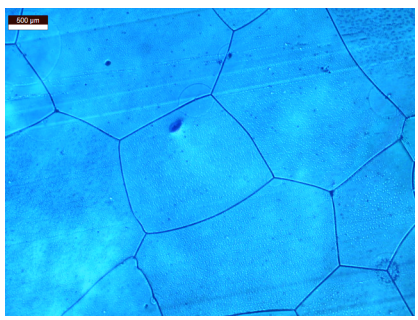

FIG. 3. Light microscope image of as-fabricated, polycrystalline "standard" ice used for both friction and creep experiments in this study.

and abraded surface roughness of the ice, as well as the plastic standards described in Section IV. Measurements were taken in two directions in at least five swaths. The abraded surfaces of standard ice had an average R_a of 7 ± 1 μm. The rocks used to simulate glacial bedrock for these experiments were medium-grained Barre granite ($50 \times 50 \times 30$ mm). The blocks were milled on a surface grinder and had an average R_a of 2.8 ± 2 μm.

III. MEASUREMENTS AND CALIBRATIONS

A. Apparatus stiffness

The vertical stiffness of the apparatus was assessed by replacing the samples with placeholders and measuring the deflection of the frame near the vertical piston when load was applied. Defined in terms of the shear stress on the double direct shear specimen (spread over two 50×50 mm sliding surfaces), the stiffness is 8.3 MPa/mm. Stiffness of the apparatus is important for friction studies because an apparatus that is too stiff relative to the material being tested will not allow stick-slip behavior to occur. Because this apparatus will be used for both stable sliding and stick-slip studies, this stiffness is in a good range to access both of those behaviors.

B. Preliminary friction experiments methodology

Our preliminary ice-on-rock friction experiments were conducted at constant normal stress in the range of 100-200 kPa and at two temperatures (−6 °C and −3 °C). Two types of basic measurements were conducted to test the efficacy of the rig. The first test performed was a velocity-stepping friction experiment, which provides both the average coefficient of friction and the rate and state variables D_C, a, and b (from Eq. (1) and Fig. 4 inset). In these experiments, a constant velocity was imposed on the sliding sample. A sudden jump in velocity was then imposed and the frictional response of the sliding sample was measured. The initial jump in friction, known as the direct effect, is a function of a. This is followed by an evolutionary decrease in friction which is a function of b and the slip distance over which friction evolves back to steady-state, D_C.

The second test was a slide-hold-slide experiment, commonly used in rock mechanics to estimate frictional healing rate (e.g., Marone, 1998). For these tests, a constant load velocity of 10 μm/s was imposed and then stopped for increasing durations: 1 s, 3 s, 10 s, 30 s, 100 s, 300 s, and 1000 s, an example of which is shown in Fig. 4. The total duration of testing was ~40 min, during which the temperature at all thermocouples held constant (bottom of Fig. 4).

C. Preliminary creep experiments methodology

A preliminary creep experiment was performed to test the apparatus' performance in load control over prolonged periods. A single steel block was moved to the center of the cryostat and superglued to the base as a bottom foundation for the ice sample (Fig. 2(c)). In order to prevent tipping of the

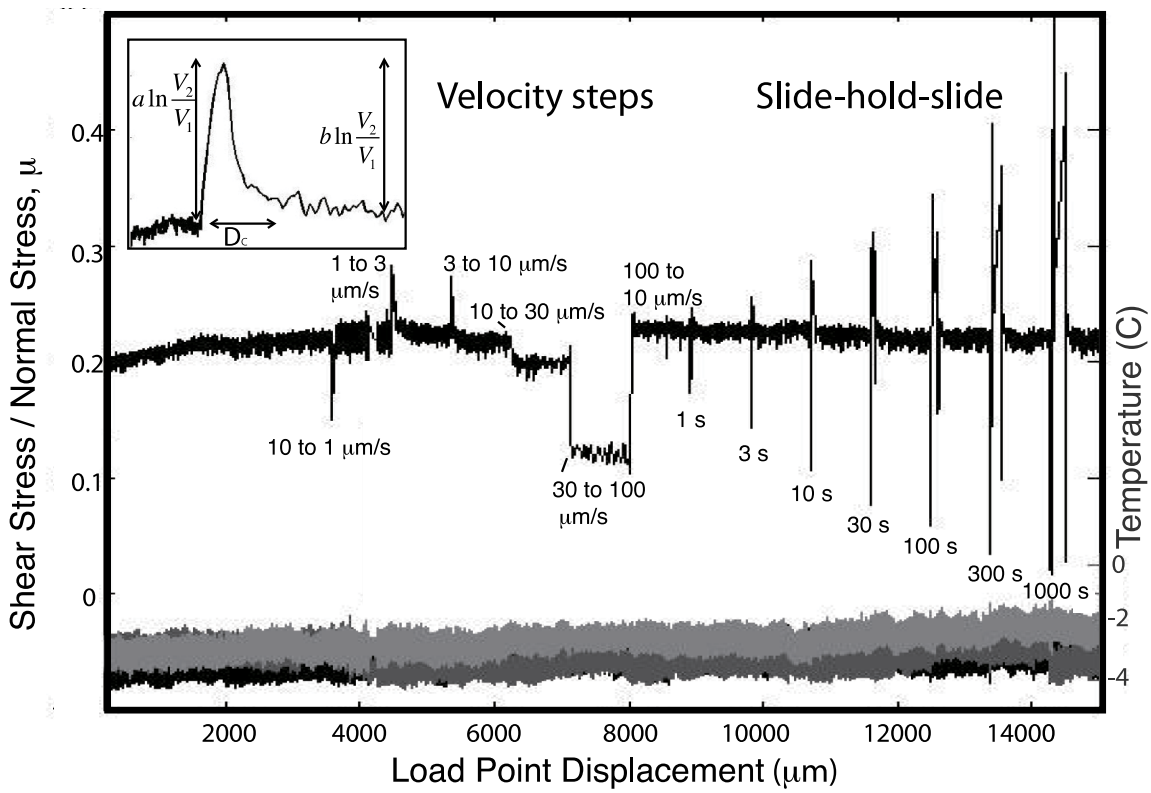

FIG. 4. Friction vs. displacement curve for ice-on-rock at -3 ± 1.8 °C. A series of 6 velocity steps are followed by slide-hold-slide experiments. An increase in peak friction is observed as hold time increases, consistent with frictional healing. Temperatures measured by thermocouples during the experiment are shown at the bottom. Lightest gray is the embedded thermocouple, medium gray sits in air below the sample, and black above the sample. The inset shows the rate-state parameters described in Section I B 1.

sample during loading, a droplet of water was placed on the pre-chilled base and then the sample affixed to this. Using the same rectangular samples of standard ice ($50 \times 50 \times 100$ mm), a constant load was applied and the shortening of the sample was measured by the motion of the vertical piston. Temperature of testing was −10 °C. The effective viscosity was determined by the slope of the strain vs. time curve after steady-state was attained (~3 h).

IV. RESULTS

A. Friction of testing standards

For the calibration of the apparatus, slider samples of various plastics with known frictional values were prepared and measured. Teflon™ (Polytetrafluoroethylene), Nylon6.6, and PMMA (polymethyl methacryliate, aka acrylic, Plexiglas, or Perspex) were chosen because they cover a spectrum of friction coefficients. PMMA has been used recently in a number of geologic papers due to its similar behavior to rocks (e.g., Rubinstein *et al.*, 2004 and Capozza *et al.*, 2011). A single rectangular block ($50 \times 50 \times 100$ mm) of each plastic was cut and the sliding interfaces prepared as follows: the PMMA was roughened with #100 grit abrasive that resulted in a roughness R_a of 1.7 ± 0.2 μm; the Nylon was tested as received, with an R_a of 2.8 ± 0.7 μm; the Teflon was polished incrementally down to #600 grit and resulted in an R_a of 0.5 ± 0.1 μm. Tests were conducted at room temperature. Nylon6.6 and PMMA were tested against rock; Teflon was tested against itself. We applied various normal loads and drove the upper piston a known load point velocity. The shear stress responded according to the friction of each material. Friction is calculated from the ratio of the shear stress to the normal stress. Figure 5 shows the results from tests on these standards, which are consistent with published results (Lee and Golden, 1988; Biswas and Vijayan, 1992; Pouzada *et al.*, 2006; Omega Engineering Technical Reference, 2000; and Blackford *et al.*, 2012). The PMMA demonstrated very different tribology from the other plastics. As shown in Fig. 6 it displayed clear stick-slip behavior. The amplitude of shear stress drops decreased with increasing load point velocity (inset), so that experimental studies performed at very high velocities (>8000 μm/s) probably observed no stick-slips (Lee and Golden, 1988).

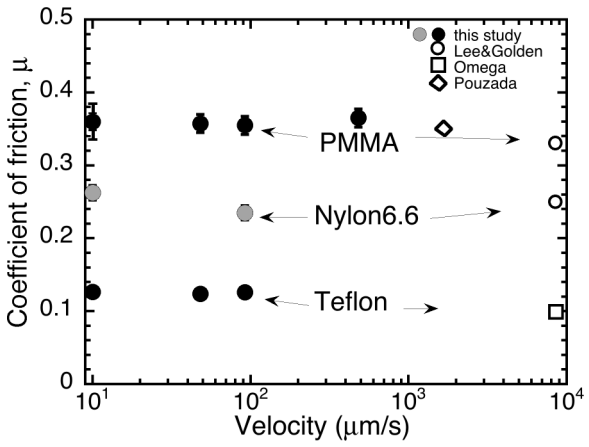

FIG. 5. Friction coefficient vs. sliding velocity for various plastics tested at room temperature. Normal loads were as follows: (1) PMMA at 60 kPa; (2) Nylon at 114 kPa; Teflon at 400 kPa. The data from this study (closed symbols) are compared to previous studies (open symbols). For this study, PMMA and Nylon were tested against rock. The PMMA surface roughness, R_a, was 1.7 ± 0.2 μm and Nylon R_a was 2.8 ± 0.7 μm. Teflon was tested against itself and its R_a was 0.5 ± 0.1 μm. Where error bars are not visible, they are smaller than the symbol size.

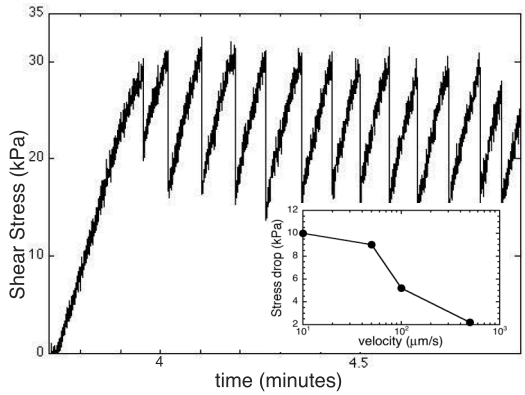

FIG. 6. Shear stress over time for PMMA tested against rock at $\sigma_n = 60$ kPa and room temperature. Stick-slip behavior is observed at 10 μm/s. Inset: the drop in shear stress associated with each slip decreases with velocity.

B. Friction of ice

Figure 7 shows the stable sliding friction coefficient μ as a function of sliding velocity for polycrystalline ice sliding on rock at two temperatures (−6 and −3 ± 1.8 °C). In all cases, the normal stress was 100-200 kPa. The data are compared to previously published results from ice tested at the same temperatures, but higher normal stress (σ_n = 1 MPa; Zoet *et al.*, 2013). A decrease in friction with increasing temperature is observed. As seen in Fig. 3, slide-hold-slide experiments revealed significant frictional healing that increased with hold time, as indicated by the spike in shear stress following each hold. This phenomena and other rate-state parameters will be

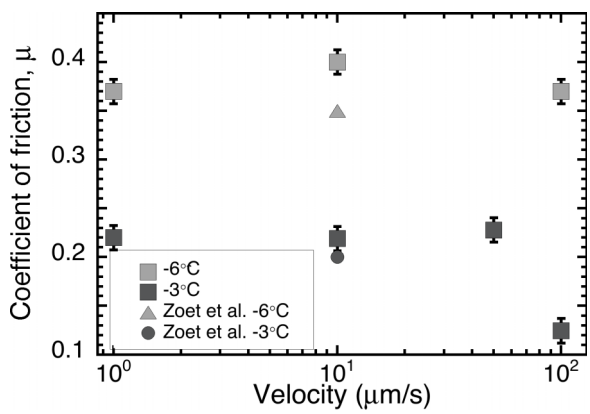

FIG. 7. Friction coefficient of polycrystalline ice against rock at various temperatures with σ_n = 100-200 kPa. Error bars represent the range of noise in the τ/σ_n data. Error in temperature is determined by manufacturer at ±1.8 °C. The data are compared to a published study of ice on rock tested with σ_n = 1 MPa (Zoet *et al.*, 2013).

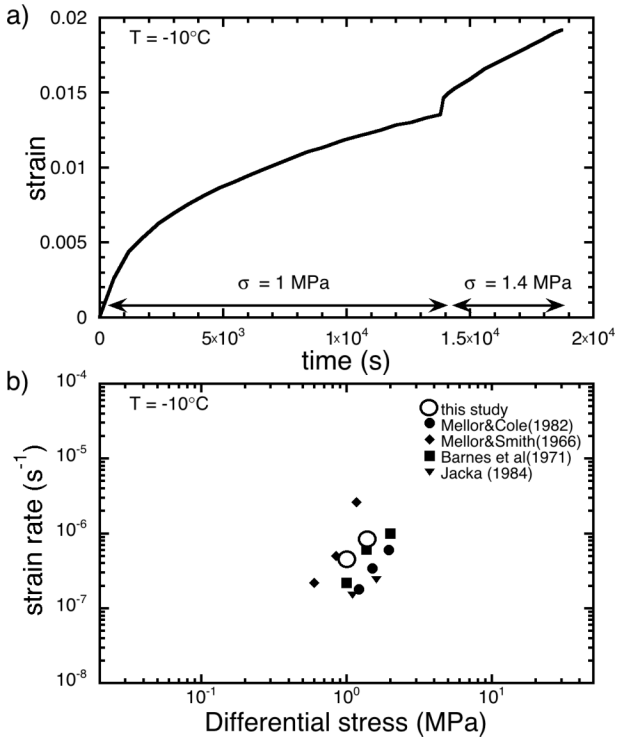

FIG. 8. (a) Unidirectional creep data for polycrystalline ice with a grain size of ~1.5 mm tested at −10 ± 1.8 °C at two stress steps: 1 MPa and 1.4 MPa. For this initial study, load was applied gradually. Zero point in time and strain in this figure were arbitrarily set to the moment 1 MPa was reached. (b) Logarithmic stress vs. strain rate for two curves shown in (a) compared to previous studies. [Mellor and Cole, 1982; Mellor and Smith, 1966; Barnes *et al.*, 1971; and Jacka, 1984].

explored in greater detail in future studies. These preliminary studies demonstrate that the apparatus is fully capable of conducting frictional experiments on ice.

C. Viscosity of ice

Figure 8 shows unidirectional (steady-state) creep data for ~1.5 mm grain size polycrystalline ice at constant temperature (−10 ± 1.8 °C) at two applied stresses (1 MPa and 1.4 MPa). Since the first load step was applied gradually over the course of 1 h—and over 2 min for the second load step—the obtained creep curves (Fig. 8(a)) cannot be used to analyze the elastic or transient response (which require an instantaneous application of stress), but the steady-state portions of each stress step were analyzed for strain rate. A logarithmic plot of stress vs. strain rate (Fig. 8(b)) demonstrates that the results of our study are consistent with previous studies on ice at the same conditions. That the results are slightly higher than previous studies is probably due to the brevity of these preliminary tests; true steady-state might not have been reached.

V. CONCLUSIONS

In this paper, we describe a new apparatus and preliminary tests to measure various deformation behaviors of polycrystalline ice. Our results demonstrate the ability to recreate previous studies. Future studies will explore conditions outside of currently published ranges, including frequency and amplitude dependences of oscillatory loads and the effects of secondary phases and crystallographic fabrics. The combination of precise, servo-controlled stress and displacement along the sample with precise temperature control over a wide range of cold temperatures represents a significant step forward for ice deformation experiments.

ACKNOWLEDGMENTS

This apparatus was initially built using seed money from the LDEO Innovation Fund. Research and testing was supported by the Brinson Foundation, by NASA under Award No. NNX13AL01G, and by NSF under Award No. ANT 1245871. The authors thank Sabrina Bellantoni for her assistance with roughness measurements and calibrations. Lamont-Doherty contribution number 8012.

Adalgeirsdottir, G., Smith, A. M., Murray, T., King, M., Makinson, K., Nicholls, K. W., and Behar, A. E., "Tidal influence on Rutford Ice Stream, West Antarctica: Observations of surface flow and basal processes from closely spaced GPS and passive seismic stations," J. Glaciol. **54**(187), 715–724 (2008).

Barnes, P., Tabor, D., and Walker, J. C. F., "The friction and creep of polycrystalline ice," Proc. R. Soc. A **324**, 127–155 (1971).

Beeler, N. M. and Lockner, D. A., "Why earthquakes correlate weakly with the solid Earth tides: Effects of periodic stress on the rate and probability of earthquake occurrence," J. Geophys. Res. **108**(B8), 2391, doi:10.1029/2001JB001518 (2003).

Biswas, S. K. and Vijayan, K., "Friction and wear of PTFE——A review," Wear **158**, 193–211 (1992).

Blackford, J. R., Skouvaklis, G., Purser, M., and Koutsos, V., "Friction on ice: Stick and slip," Faraday Discuss. **156**(1), 243–254 (2012).

Bowden, F. P. and Hughes, T. P., "The mechanism of sliding on ice and snow," Proc. R. Soc. A **172**(949), 280–298 (1939).

Capozza, R., Rubinstein, S. M., Barel, I., Urbakh, M., and Fineberg, J., "Stabilizing stick-slip friction," Phys. Rev. Lett. **107**, 024301 (2011).

Cole, D. M., "Preparation of polycrystalline ice specimens for laboratory experiments," Cold Reg. Sci. Technol. **1**, 153–159 (1979).

Cole, D. M., "A model for the anelastic straining of saline ice subjected to cyclic loading," Philos. Mag. A **72**(1), 231–248 (1995).

deJuan, J., Elosegui, P., Nettles, M., Larsen, T. B., Davis, J. L., Hamilton, G. S., Stearns, L. A., Anderson, M. L., Ekstrom, G., Ahlstrom, A. P., Stenseng, L., Khan, S. A., and Forsberg, R., "Sudden increase in tidal response linked to calving and acceleration at a large Greenland outlet glacier," Geophys. Res. Lett. **37**, L12501, doi:10.1029/2010gl043289 (2010).

Dieterich, J. H., "Time-dependent friction in rocks," J. Geophys. Res. **77**, 3690–3697, doi:10.1029/JB077i020p03690 (1972).

Dieterich, J., "A constitutive law for rate of earthquake production and its application to earthquake clustering," J. Geophys. Res. **99**(B2), 2601–2618, doi:10.1029/93JB02581 (1994).

Durham, W. B., Heard, H. C., and Kirby, S. H., "Experimental deformation of polycrystalline H_2O ice at high pressure and low temperature: Preliminary results," J. Geophys. Res. **88**, B377–B392, doi:10.1029/JB088iS01p0B377 (1983).

Durham, W. B., Stern, L. A., and Kirby, S. H., "Rheology of ice I at low stress and elevated confining pressure," J. Geophys. Res. **106**(6), 11031–11042, doi:10.1029/2000JB900446 (2001).

Durham, W. B., Stern, L. A., Kubo, T., and Kirby, S. H., "Flow strength of highly hydrated Mg- and Na-sulfate hydrate salts, pure and in mixtures with water ice, with application to Europa," J. Geophys. Res. **110**, E12010, doi:10.1029/2005JE002475 (2005).

Duval, P., Ashby, M. F., and Anderman, I., "Rate-controlling processes in the creep of polycrystalline ice," J. Phys. Chem. **87**, 4066–4074 (1983).

Fortt, A. L. and Schulson, E. M., "Frictional sliding across Coulombic faults in first-year sea ice: A comparison with freshwater ice," J. Geophys. Res.: Oceans **116**(C11), C11012, doi:10.1029/2011JC006969 (2011).

Golding, N., Burks, C. E., Lucas, K. N., Fortt, A. L., Snyder, S. A., and Schulson, E. M., "Mechanical properties of the ice I-magnesium sulfate eutectic: A comparison with freshwater ice in reference to europa," Icarus **225**, 248–256 (2013).

Goldsby, D. L. and Kohlstedt, D. L., "Superplastic deformation of ice: Experimental observations," J. Geophys. Res. **106**, 11017–11030, doi:10.1029/2000JB900336 (2001).
Gudmundsson, A. G. H., "Tides and the flow of Rutford Ice Stream, West Antarctica," J. Geophys. Res. **112**, F04007, doi:10.1029/2006JF000731 (2007).
Hoskins, E. R., Jaeger, J. C., and Rosengren, K. J., "A medium-scale direct friction experiment," Int. J. Rock Mech. Min. Sci. **5**, 143–154 (1968).
Jacka, T. H., "The time and strain required for development of minimum strain rates in ice," Cold Reg. Sci. Technol. **8**(3), 261–268 (1984).
Kennedy, F. E., Schulson, E. M., and Jones, D. E., "The friction of ice on ice at low sliding velocities," Philos. Mag. A **80**(5), 1093–1100 (2000).
Lee, M. C. H. and Golden, M. A., "The coefficient of friction of a polyamide/polymethyl methacrylate blend system," J. Elastomers Plast. **20**, 163–186 (1988).
Lishman, B., Sammonds, P., and Feltham, D., "A rate and state friction law for saline ice," J. Geophys. Res. **16**, C05011, doi:10.1029/2010jc006334 (2011).
Lockner, D. A. and Beeler, N. M., "Premonitory slip and tidal triggering of earthquakes," J. Geophys. Res. **104**(B9), 20133–20151, doi:10.1029/1999JB900205 (1999).
Maeno, N., Arakawa, M., Yasutome, A., Mizukami, N., and Kanazawa, S., "Ice-ice friction measurements, and water lubrication and adhesion-shear mechanisms," Can. J. Phys. **81**, 241–249 (2003).
Marone, C., "The effect of loading rate on static friction and the rate of fault healing during the earthquake cycle," Nature **391**, 69–72 (1998).
McCarthy, C., Cooper, R. F., Goldsby, D. L., Durham, W. B., and Kirby, S. H., "Transient and steady state creep response of ice I and magnesium sulfate hydrate eutectic aggregates," J. Geophys. Res. **116**, E04007, doi:10.1029/2010je003689 (2011).
McCarthy, C. and Cooper, R. F., "Tidal dissipation in creeping ice and the thermal evolution of Europa," Earth Planet. Sci. Lett. **443**, 185–194 (2016).
Mellor, M. and Smith, J. H., "Creep of snow and ice," Cold Regions Research & Engineering Lab Research Report, Volume 220, 13pp., 1966.
Mellor, M. and Cole, D., "Deformation and failure of ice under constant stress or constant strain rate," Cold Reg. Sci. Technol. **5**(2), 201–219 (1982).
Nimmo, F., Spencer, J. R., Pappalardo, R. T., and Mullen, M. E., "Shear heating as the origin of the plumes and heat flux on Enceladus," Nature **447**, 289–291 (2007).
Omega Engineering Technical Reference, PFA flurorocarbon Resin information, omega.com, 2000.
Pouzada, A. S., Ferreira, E. C., and Pontes, A. J., "Friction properties of moulding thermoplastics," Polym. Test. **25**, 1017–1023 (2006).
Ruina, A. L., "Slip instability and state variable friction laws," J. Geophys. Res. **88**, 10359–10370, doi:10.1029/JB088iB12p10359 (1983).
Rubinstein, S. M., Cohen, G., and Fineberg, J., "Detachment fronts and the onset of dynamic friction," Nature **430**, 1005–1009 (2004).
Savage, H. M. and Marone, C., "Effects of shear velocity oscillations on stick-slip behavior in laboratory experiments," J. Geophys. Res. **112**, B02301, doi:10.1029/2005jb004238 (2007).
Savage, H. M. and Marone, C., "Potential for earthquake triggering from transient deformations," J. Geophys. Res. **113**(B5), doi:10.1029/2007jb005277 (2008).
Schindelin, J., Arganda-Carreras, I., Frise, E., Kaynig, V., Longair, M., Pietzsch, T., Preibisch, S., Rueden, C., Saalfeld, S., Schmid, B., and Tinevez, J. Y., "Fiji: An open-source platform for biological-image analysis," Nat. Methods **9**(7), 676–682 (2012).
Schneider, C. A., Rasband, W. S., and Eliceiri, K. W., "NIH image to ImageJ: 25 years of image analysis," Nat. Methods **9**(7), 671–675 (2012).
Schulson, E. M. and Fortt, A. L., "Friction of ice on ice," J. Geophys. Res. **117**, B12204, doi:10.1029/2012JB009219 (2012).
Shoji, D., Hussman, H., Kurita, K., and Sohl, F., "Ice rheology and tidal heating of Enceladus," Icarus **226**, 10–19 (2013).
Singer, K. N., McKinnon, W. B., Schenk, P. M., and Moore, J. M., "Massive ice avalanches on Iapetus mobilized by friction reduction during flash heating," Nat. Geosci. **5**, 574–578 (2012).
Tatibouet, J., Perez, J., and Vassoille, R., "Study of grain boundaries in ice by internal friction measurement," J. Phys. **48**, 197–203 (1987).
van der Elst, N. J. and Savage, H. M., "Frequency dependence of delayed and instantaneous triggering on laboratory and simulated faults governed by rate and state friction," J. Geophys. Res.: Solid Earth **120**, 3406–3429, doi:10.1002/2014JB011611 (2015).
Wiens, D. A., Anandakishnan, S., Winberry, J. P., and King, M. A., "Simultaneious teleseismic and geodetic observations of the stick-slip motion of an Antarctic ice stream," Nat. Lett. **453**, 770–775 (2008).
Winberry, J. P., Anandakrishnan, S., Alley, R. B., Bindschadler, R. A., and King, M. A., "Basal mechanics of ice streams: Insights from the stick-slip motion of Whillans Ice Stream, West Antarctica," J. Geophys. Res. **114**, F01016, doi:10.1029/2008JF001035 (2009).
Winberry, J. P., Anandakrishnan, S., Wiens, D. A., Alley, R. B., and Christianson, K., "Dynamics of stick-slip motion, Whillans Ice Stream, Antarctica," Earth Planet. Sci. Lett. **305**, 283–289 (2011).
Zoet, L. K., Anandakrishnan, S., Alley, R. B., Nyblade, A. A., and Wiens, D. A., "Motion of an Antarctic glacier by repeated tidally modulated earthquakes," Nat. Geosci. **5**, 623–626 (2012).
Zoet, L. K., Carpenter, B., Scuderei, M., Alley, R. B., Anandakrishnan, S., Marone, C., and Jackson, M., "The effects of entrained debris on the basal sliding stability of a glacier," J. Geophys. Res. **118**, 656–666, doi:10.1002/jgrf.20052 (2013).